CFD Analysis of NACA 64A-206 Airfoil in Supersonic Flow

Muhammad Abdullah Zafar Ghauri[1]

[1]School of Mechanical and Manufacturing Engineering (SMME), NUST, Islamabad

[1]mghauri.ug22smme@student.nust.edu.pk

Abstract*— The report focuses on numerical analysis of aerodynamic characteristics of the NACA 64A-206 airfoil for turbulent flow at compressible and high Mach number using Computational Fluid Dynamics (CFD). Different Reynolds numbers have been chosen for analysis, for which the angles of attack are unique. Scenarios for analysis are simple state, shockwave state and stalling state, with maximum angles of attack dominating the stalling effect and minimum angle of attacks dominating the shockwave state. The fluid is taken into account to be steady state, two dimensional, ideal and compressible in nature. The simulations were done using the Ansys Fluent 2023R2 Student Version. Reynolds averaged Navier-Stokes (RANS) served the source for obtaining the desired answers, and for resolving of the flow turbulence, the k-ω SST turbulence model was selected in addition to the Spalart-Allmaras Model (S-A Model, set as vorticity-based modelling) which served to explicitly deliberate over the shockwave case.

Keywords*— NACA, Computational Fluid Dynamics (CFD), Reynolds averaged Navier-Stokes, Spalart-Allmaras Turbulent Modelling, SST k-ω Turbulent Modelling, Ansys Fluent

I. INTRODUCTION

Airfoil sections have been developed during 1800s. Mainly the study of airfoil sections depends on boundary layer theory developed by Ludwig Prandtl, having mentioned in his theoretical analysis that the fluid flowing over an object is divided and flows as two regions, respectively as the laminar region, which is outside flow region, and the region closer to the object, due to surface friction the flow to moving slowly. This in turn causes the air to flow at different velocities at the lower and upper surface of the object that comes in the flow of air.

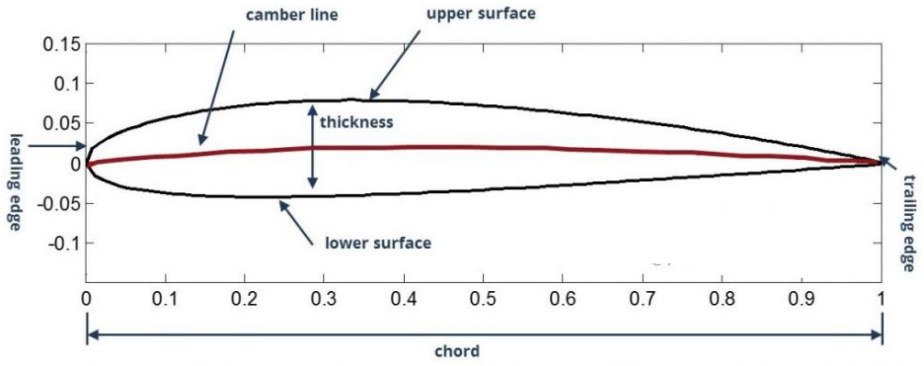


Figure 1 General Airfoil Nomenclature

Bringing into consideration a general airfoil, the front of the airfoil is referred to as the leading edge and the rear the trailing edge. The airfoil upper and lower surfaces coincide at the leading and trailing edges.

The length of the airfoil from leading to trailing edge is known as the airfoil chord. This often varies down the span of the wing as the wing tapers from the root to the tip. Camber is an important parameter in an airfoil which is the measure of the asymmetry between the upper and lower surface. The main purpose for its introduction to increase its maximum lift coefficient, which in turn decreases the stall speed of the aircraft. The camber line is a line drawn equidistant between the upper and lower surface at all points along the chord.

NACA 64A-206 has a standardized four-digit profile, which is developed by National Advisory Committee for Aeronautics. Generally, for the F-16 and training jets, NACA 64A-206 airfoil is brought into consideration because of the fact that the specified airfoil during the flight, the F-16 has an ability to change the geometry of its wings, and thus its airfoil geometric characteristics, by deflecting the leading or trailing edge flaps or both. By doing so the wing effectively changes the curvature and the camber line of the airfoil. And since the curvature and camber line have a significant impact on the airfoil characteristics, it results in changes in lift, drag and pressure coefficients. At supersonic speed the F-16 automatic device schedule includes leading and trailing edges with a negative deflection

Table 1 NACA 64A-206 Coordinates

NACA 64A206			
(Stations and ordinates given in per cent of airfoil chord)			
Upper Surface		Lower Surface	
Station	Ordinate	Station	Ordinate
0.95007	0	0	0.0000
0.90015	0.00541	-0.00442	-0.2791
0.8502	0.00796	-0.00524	-0.3233
0.80024	0.01302	-0.00645	-0.3833
0.75025	0.0256	-0.00836	-0.4738
0.70023	0.05066	-0.01087	-0.5747
0.6502	0.07568	-0.01267	-0.6369
0.60015	0.10067	-0.0141	-0.6825
0.55008	0.15063	-0.01624	-0.7411
0.5	0.20057	-0.01775	-0.7734
0.44991	0.25048	-0.01877	-0.7854
0.39981	0.30039	-0.01935	-0.7803
0.34971	0.35029	-0.01951	-0.7591
0.29961	0.40019	-0.01924	-0.7196
0.24952	0.45009	-0.01824	-0.6511
0.19943	0.5	-0.01672	-0.5580
0.14937	0.54992	-0.0148	-0.4490
0.09933	0.59985	-0.0126	-0.3317
0.07432	0.6498	-0.0102	-0.2121
0.04934	0.69977	-0.00768	-0.0965
0.0244	0.74975	-0.00517	0.0041
0.01198	0.79976	-0.00276	0.0700
0.00704	0.8498	-0.00064	0.0702
0.00459	0.89985	0.00094	0.0518
0	0.94993	0.00159	0.0241

II. METHODOLOGY

For the sake of CFD analysis of NACA 64_A-206 Airfoil, ANSYS Fluent Student Version 2023 was used to solve Reynolds Averaged Navier Stokes equations (RANS), which ultimately are based on the basic concepts of conservation of mass, momentum, and energy equations. For the general analysis, K-ω Turbulence Model and Spalart-Allmaras Vorticity Model (S-A model) were brought into consideration. S-A model was brought into consideration owing to fast convergence rate with relatively less computational cost and conveniency.
Referring to the Equation of Continuity, which is expressed as:

$$\frac{\partial \rho}{\partial t} + \nabla.(\rho\overrightarrow{u}) = 0$$

Equation 1 Continuity Equation

The first and second term in Eqn.(1) represent the change rate in mass through an element of control volume and the change rate in mass due to convection, respectively.
Considering the Momentum Equation, which is expressed in terms as:

$$\frac{\partial}{\partial t}(\rho\overrightarrow{u}) + \nabla(\rho\overrightarrow{uu}) = -\nabla P + \nabla(\bar{\bar{\tau}}) + \rho\bar{g}$$

Equation 2 Momentum Equation

The first, second, third, fourth, and fifth term in Eq.(2) represent the change rate in momentum through an element of control volume, momentum due to convection, pressure forces, viscous forces, and gravitation, respectively.

Referring to another crucial equation, which is the Energy Equation:

$$\rho c_p \left(\frac{\partial T}{\partial t} + v_x\frac{\partial t}{\partial x} + v_y\frac{\partial T}{\partial y}\right)=\lambda \left(\frac{\partial^2 T}{\partial x^2} + \frac{\partial^2 T}{\partial y^2}\right)$$

Equation 3 Energy Equation

The aforementioned Eq. (3) represents the equation of energy which is applied when heat transfer or pressure is existed in the flow. Considering the airfoil analysis, the flow of fluid (air) is assumed to be Newtonian and incompressible.

$$\frac{\partial}{\partial t}(\rho k) + \frac{\partial}{\partial x_i}(\rho k u_i)= \frac{\partial}{\partial x_i}\left(\alpha_k u_\varepsilon \frac{\partial k}{\partial x_i}\right) + G_k + G_b + Y_M + S_k + \rho\varepsilon$$

Equation 4 k-ω Turbulence Modelling Equation

$$\frac{\partial}{\partial t}(\rho\varepsilon) + \frac{\partial}{\partial x_i}(\rho\varepsilon u_i)= \frac{\partial}{\partial x_i}\left(\alpha_k u_\varepsilon \frac{\partial \varepsilon}{\partial x_i}\right)+G_{1\varepsilon}\frac{\varepsilon}{k}(G_k + C_{3\varepsilon}C_b) - C_{2\varepsilon}\frac{\varepsilon^2}{k} - R_\varepsilon + S_\varepsilon$$

Equation 5 k-ε Turbulence Modelling Equation

Considering the investigation for said airfoil, at High Reynolds Number, k-ω RNG Model is brought into consideration as verified by turbulence model dependency analysis.
For *k-ω* RNG Turbulence model, the turbulence kinetic energy, k and its rate of dissipation *ε*, in *k-ε* RNG turbulence model can be found.
Considering the Eq.(4) G_k and G_b represent the turbulence kinetic energy generation resulted from velocity gradient, buoyancy, respectively. Y_m is the oscillating dilation contribution in the case of compressible turbulence. α_ε and α_k are the inversely Prandtl numbers for ε and k, respectively.
The Spalart-Allmaras model, being specifically developed for aerospace applications which predominantly involve wall-bounded flows, is basically a single equation which helps in evaluating a modelled transport equation for the kinematic eddy turbulent viscosity. As far as results are concerned, it produces good results for boundary layers subjected to adverse pressure gradients. It is also gaining popularity in turbomachinery applications. It was developed for aerodynamic flows, while it produces no errors for free shear flows which dominate for planes and air jets. When existing in true form, it is generally effective in cases involving relatively small values of Reynolds numbers, hence making it compulsory for the region affected by effects of viscosity to be resolved in an adequate manner (y+~1 meshes).
It solves a transport equation for a viscosity-like variable $\tilde{\nu}$which may be referred to as the Spalart–Allmaras variable.

$$\frac{\partial \hat{\nu}}{\partial t}+u_j\frac{\partial \hat{\nu}}{\partial x_j} = c_{b1}(1-f_{t2})\hat{S}\hat{\nu}-\left[c_{w1}f_w - \frac{c_{b1}}{\kappa^2}f_{t2}\right]\left(\frac{\hat{\nu}}{d}\right)^2+\frac{1}{\sigma}\left[\frac{\partial}{\partial x_j}\left((\nu+\hat{\nu})\frac{\partial \hat{\nu}}{\partial x_j}\right) + c_{b2}\frac{\partial \hat{\nu}}{\partial x_i}\frac{\partial \hat{\nu}}{\partial x_i}\right]$$

Equation 6 Spalart-Allmaras Turbulence Model Equation

and the turbulent eddy viscosity is computed from:

$$\mu_t = \rho\hat{\nu}f_{v1}$$

Equation 7 Turbulence Eddy Viscosity

For which,

$$f_{v1} = \frac{\chi^3}{\chi^3 + c_{v1}^3}$$

And,

$$\chi = \frac{\hat{\nu}}{\nu}$$

and ρ is the density, $\nu = \mu/\rho$ is the molecular kinematic viscosity, and μ is the molecular dynamic viscosity. Additional definitions are given by the following equations:

$$\hat{S} = \Omega + \frac{\hat{\nu}}{\kappa^2 d^2}f_{v2}$$

Where,

$$\Omega = \sqrt{2W_{ij}W_{ij}}$$

Equation 8 Magnitude of Viscosity

d is the distance from the field point to the nearest wall, and

$$f_{v2} = 1 - \frac{\chi}{1 + \chi f_{v1}}$$
$$f_w = g\left[\frac{1 + c_{w3}^6}{g^6 + c_{w3}^6}\right]^{1/6}$$
$$g = r + c_{w2}(r^6 - r)$$
$$r = min\left[\frac{\hat{\nu}}{\hat{S}\kappa^2 d^2}, 10\right]$$
$$f_{t2} = c_{t3} exp\left(-c_{t4}\chi^2\right)$$
$$W_{ij} = \frac{1}{2}\left(\frac{\partial u_i}{\partial x_j} - \frac{\partial u_j}{\partial x_i}\right)$$

The constants used in the aforementioned detailed equations can be enumerated as follows:

Table 2 Values of Constants used in Spalart-Allmares Turbulence Model Equation

Constants	Values
c_{b1}	0.135
σ	0.667
c_{b2}	0.622
κ	0.41
c_{w2}	0.3
c_{v1}	7.1
c_{t3}	1.2
c_{t4}	0.5
c_{w1}	$\frac{c_{b1}}{\kappa^2} + \frac{1 + c_{b2}}{\sigma}$ or 3.23

III. **CFD MODELLING OF FLOW PAST AIRFOIL**

Finite Volume Method is the unique numerical technique used by Ansys Fluent to solve the aforementioned equations in an efficient manner.

Initial step for CFD modelling involves the successful setup of rendered geometry, for which, in the following case, the NACA 64_A-206 coordinate data was imported from NACA website to Excel worksheet and the coordinates were demarcated in a way such that equal numbers rested for upper and lower region of airfoil after which they were imported into Ansys Design Modeler setup in the form of 3D curves and later finalized followed by generating the surface. Additional parameters are also brought into consideration, primarily being the contour generation. Contour is a closed region within which an airfoil is subjected to extremities. Afterwards, mesh controls and setup were selected. Next, solver settings and solver preference are chosen, along with the boundary and flow conditions. The selected turbulence model for resolving the flow simulation is the k-ω SST model along with the pressure-based coupling algorithm followed by comparison with S-A model swt to vorticity standards

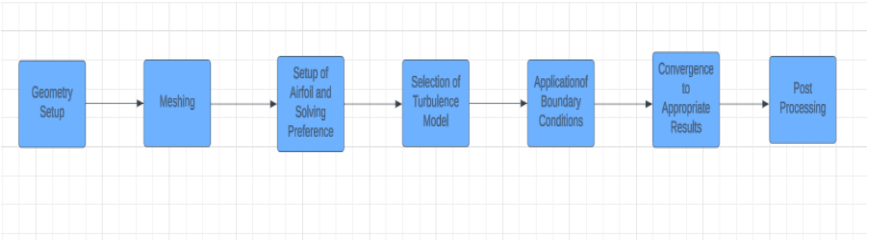


Figure 2 Flowchart for Obtaining Relevant Results using Ansys Fluent

IV. GEOMETRY SETUP

Once the coordinate file was extracted from NACA repository, it was placed in Excel worksheet where the coordinates were split accordingly in a way such that they existed separately for the upper and lower region of airfoil. Upon opening a new project in Ansys Fluent 2023, the DesignModeler, which is a CAD interface in Ansys was opened which was ultimately used to plot the airfoil in respective of provided coordinates. Following result was obtained successfully:

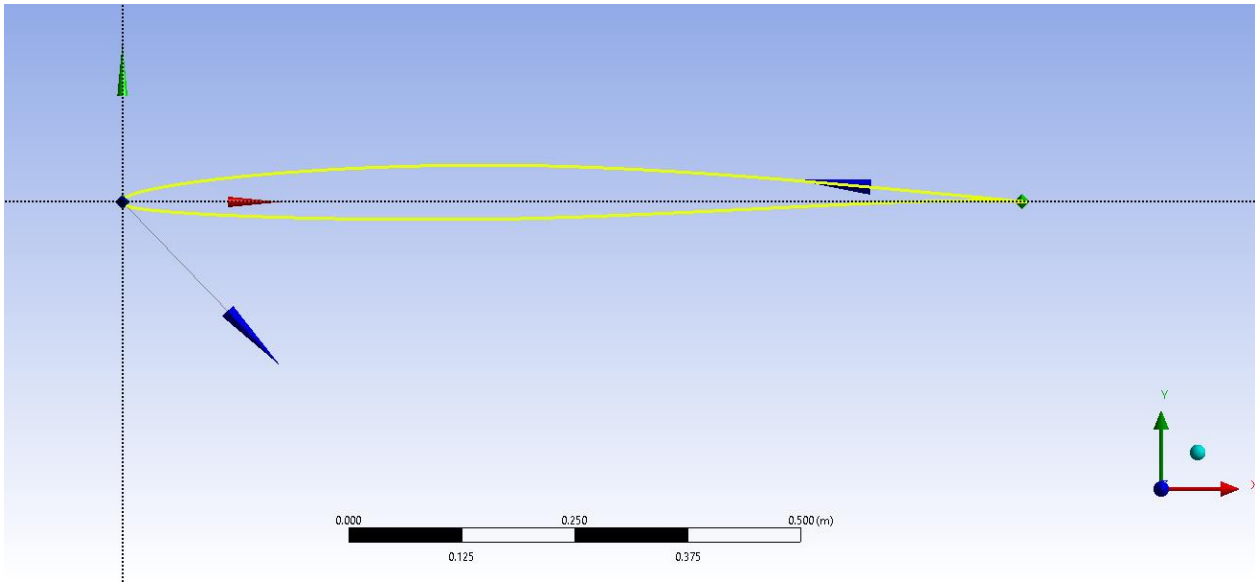


Figure 3 Generated NACA 64A-206 Airfoil

Once the airfoil was generated successfully, flow field was generated which was a closed contour for successful analysis of airfoil. Specified length values have been proven to be enough, as to not receive the reverse back flow, and other various effects which may occur if the flow field area is too small. The idea is to simulate the flow through the flow domain, and to cut out the surface of an airfoil from the flow domain, so it acts as a wall over which the free stream flows.

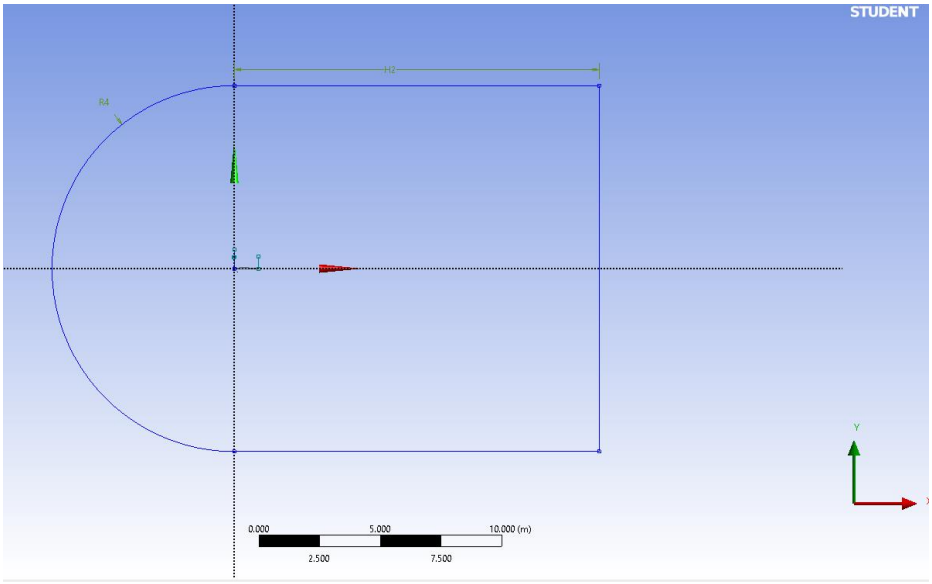


Figure 4 Airfoil enclosed within Closed Flow Field

For the following airfoil, the chord length was taken as 1m (for the sake of simplicity in best accordance with the datasheet). Two lines were sketched, one at the trailing edge and one line about 0.08m from the leading edge. The sole purpose of sketching those lines was to enhance the meshing which is to be carried out in next step.
While the semi-circular region radius was 7.5 m and the wall length was 15 m. Since the flow field was considered a fluid for analysis, surface generation was a crucial step which was rendered by creating a closed surface using Sketch command. Since the airfoil was to be analysed for the external properties, it meant that the

airfoil was to be subtracted from the generated surface, which was done so using the subtract Boolean command. The Figure 5 represents the subtracted airfoil.

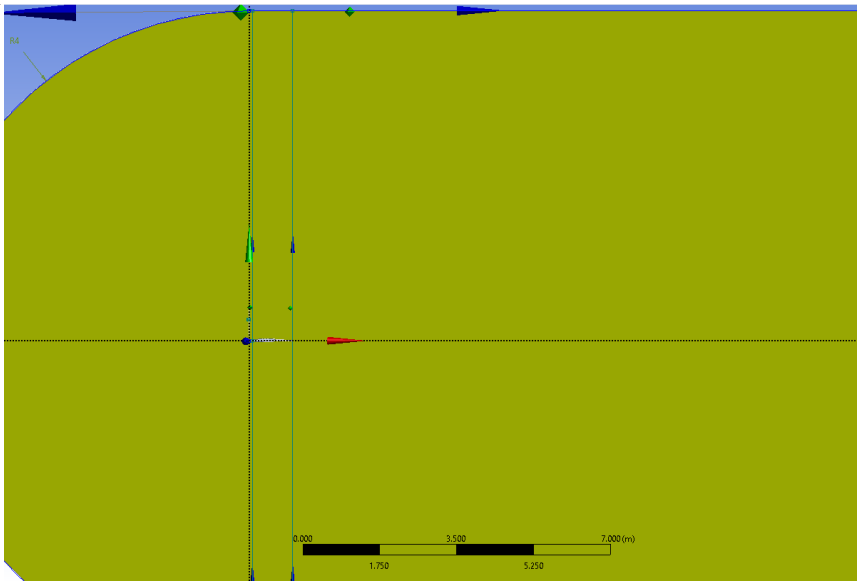


Figure 5 Airfoil enclosed in a Subtracted Closed Flow Field

In order to enhance the upcoming meshing procedure, the flow field was split into individual regions, which enumerated into six separate regions. The result was a closed surface with six different regions for future analysis.

V. MESHING

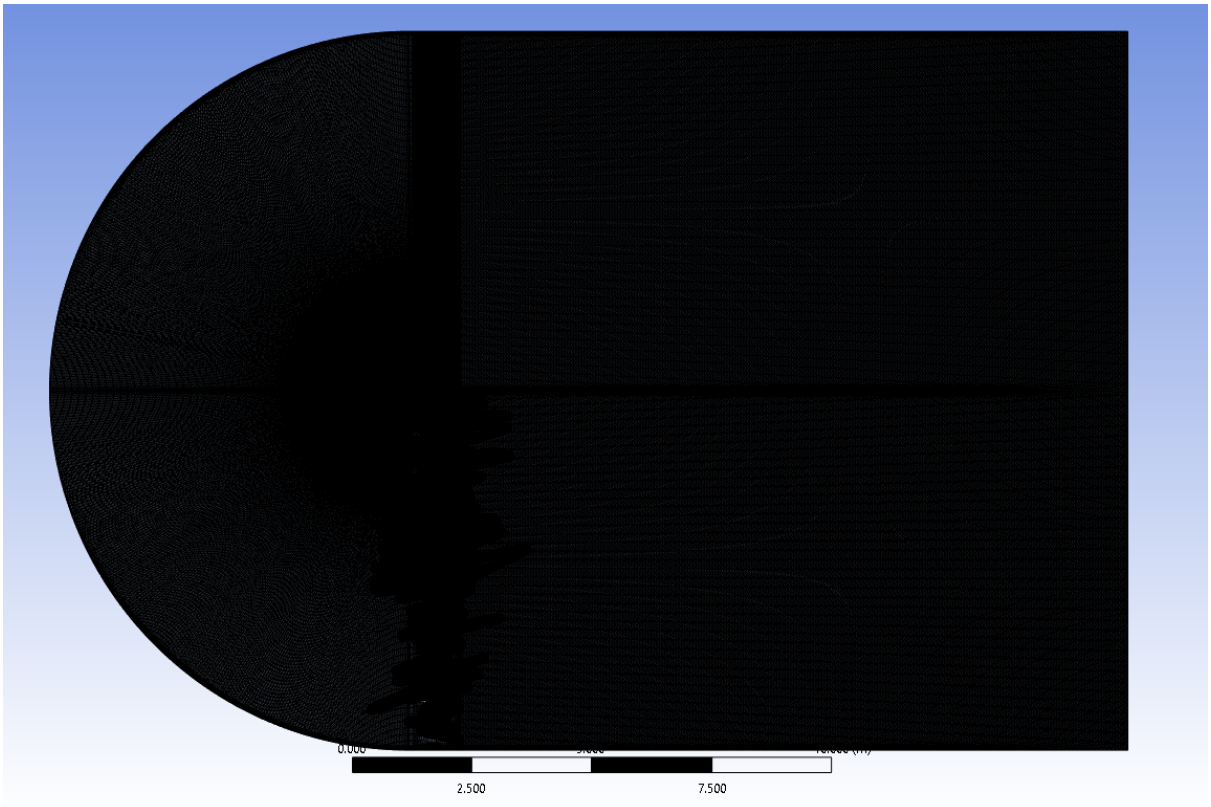


Figure 6 Quadrilateral Meshing of NACA 64A-206 Airfoil and Flow Field Region

Meshing serves an important role in CFD analysis primarily the fact that it helps in simplification of complex functions and equations into discrete blocks which are relatively easier to be dealt with. Having esteem importance in CFD and FEA, it demarcates a complex region into small block/cells. Mesh simply breaks down the object to be simulated into smaller cells that can accurately define the geometry of the object. The governing

equation can be associated with each cell, which helps in the simulation of the flow in that discrete space. With a high-quality mesh, numerical analysis can be ensured with accuracy and precision. The generated cells/blocks exist both in 2D and 3D, specifically triangular and quadrilateral in 2D case and tetrahedral, hexahedral in 3D case. A well-defined and fine mesh has the capability to visualize the regions with greater density concentration. Has the ability to yield utmost accuraye results, yet at the cost of computational time and occupancy of space. Considering the NACA 64_A-206 analysis, fine meshing was done, with the quadiltaeral meshing type choosen, considering the optimization in broader aspects. Keeping in view the fine meshing, the entire contour was split into six regions, with four regions being edge sized. Referring to the edge spacing, the region was edge spaced on four different compartments. The Edge Sizing was concerned with the separation lines about the airfoil and the front facing line and the outlet region, Edge Sizing 2 was concerned with the edge spacing for the lines following the trailing edge. Edge Sizing 3 was concerned with the edge spacing for the camber lines of airfoil and Edge Spacing 4 was concerned with the the inlet region. The Edge Sizing and Edge Sizing 2 were reverse biased respectively with bias factor of 50000 and 300 respectively, while for Edge Space 3 and 4 were unbiased.

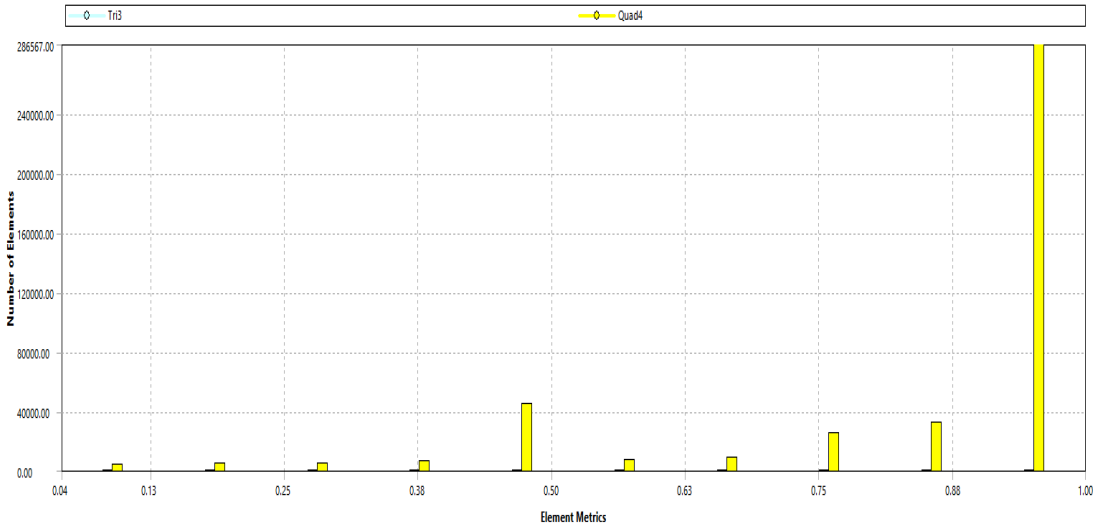


Figure 7 Mesh Quality Report demonstrating the number of quadrilaterals involved in meshing

Table 3 Mesh Report

Object Name	*Line Body*	*Surface Body*
State	Suppressed	Meshed
Graphics Properties		
Visible	No	Yes
Transparency	1	
Definition		
Suppressed	Yes	No
Model Type	Beam	Shell
Coordinate System	Default Coordinate System	
Cross Section		
Offset Mode	Refresh on Update	
Offset Type	Centroid	Middle
Treatment	None	
Dimension		3D
Stiffness Option		Membrane and Bending
Thickness		0. m
Thickness Mode		Refresh on Update
Material		
Fluid/Solid	Defined By Geometry (Solid)	
Bounding Box		
Length X	22.506 m	22.5 m

Length Y	15. m	
Length Z	0. m	
Properties		
Volume	0. m³	
Length	123.08 m	
Centroid X		4.497 m
Centroid Y		-1.0155e-006 m
Centroid Z		0. m
Surface Area(approx.)		313.32 m²
Statistics		
Nodes	0	426161
Elements	0	424872

VI. SOLUTION SETUP

Setting up an adequate solution setup is deemed a necessary step once meshing is done successfully. Any analysis which is being performed is based on some algorithm which sets forth the necessary environment and required conditions. Referring to the pressure-based approach, it was developed specifically for low-speed incompressible flows, yet the density-based approach was designed as being appropriate for high-speed compressible flows. Analysis on the broader perspective reveals that the aforementioned methods have been extended and reformulated to solve and operate for a wide range of flow conditions beyond their traditional or original intent and the velocity field for them is obtained from the momentum equations. In the pressure-based approach, the pressure field is extracted by solving a pressure or pressure correction equation which is obtained by manipulating continuity and momentum equations.

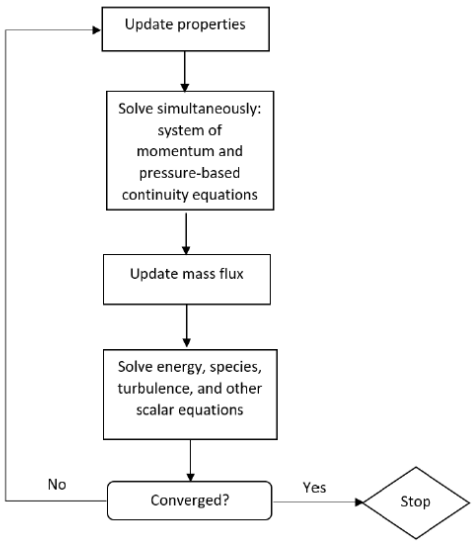


Figure 8 Algorithm/Flowchart for Computational Fluid Dynamics Analysis (Pressure Algorithm Approach)

For the convenient analysis of NACA 64A-206 airfoil, k-ω SST model has been setup, which itself is a two-equation turbulent-viscosity model, being a hybrid model which combines the k-omega and the k-epsilon models under one roof. Blending functions are adopted by the aforementioned model to establish it about near the wall and the k-ε model in the free stream. Hence affirms the fact of setting of most adequate and appropriate model for successful utilization throughout the entire flow field. Spalart-Allmaras Vorticity Turbulence Model has also been taken into account owing to single equation modelling with relatively faster convergence rate and considerably accurate results.

The governing equations tend to be the same and symmetric regardless of flow type and geometry/environment of surrounding. Yet, it is well-pertained that the flow fields are quite different for such cases, keeping in view the governing equations are the same. Boundary conditions, sometimes called the initial conditions, dictate the solutions to be obtained from the governing equations.

Keeping in regard the viscous effects of fluid flow, the boundary condition on a surface assumes zero relative velocity between the surface and the fluid immediately at the surface, which is more commonly referred to as no-slip condition.

ANSYS Fluent setup establishes and uses the Pressure far-field conditions to model a free-stream condition at infinity, with free-stream Mach number and static conditions being specified. The pressure far-field boundary condition is commonly referred to as characteristic boundary condition since it uses characteristic information (Riemann invariants) to successfully evaluate the flow variables about the boundaries.

The modelling also focuses on setting up the Spalart-Allmares Mode, within turbulence domain as vorticity model in order to analyse the shockwave case predominantly owing to the fact that generation of shockwave in k-ω turbulence model is a tedious task which is not in the domain of current analysis. Moreover, owing to the fact that the convergence rate is fast for S-A model, hence it is another main reason for analysis because CFD analysis strongly focuses on optimization of computational cost with maximum efficiency.

VII. ADJUSTMENT OF EXTERNAL PARAMETERS FOR CFD ANALYSIS

Table 4 Adjustment of External Parameters and Solution Methods

Parameters	Values
Analysis Type	Steady State
Operating Temperature	23°C
Operating Pressure	$1x10^5$ Pa
Air Density	1.225 kg/m^3
Turbulence Model	k-ω Model/Spalart-Allmaras (S-A) Model
Dynamic Viscosity (Air)	$1.802x10^{-5}$ Pa.s
Gradient	Least squared Cell Based
Pressure	Second Order
Momentum	Second Order Upwind
Turbulent Kinetic Energy	Second Order Upwind
Specific Dissipation Rate	Second Order Upwind
Pseudo Time Setup	Global Time Step
Residual Monitoring Convergence Limit	0.0001

VIII. SETUP OF ENVIRONMENT FOR EVALUATION OF SOLUTIONS AGAINST ANGLE OF ATTACKS

The most important step of CFD analysis is setting up an adequate solution environment for evaluation of adequate solutions for various angle of attacks against different values of Reynolds Numbers. For the analysis, three different Reynolds Numbers were taken into account with their respective angle of attacks to exhibit their adequate behaviour in provided conditions. The analysis was performed in Ansys Fluent Fluid Flow interface.

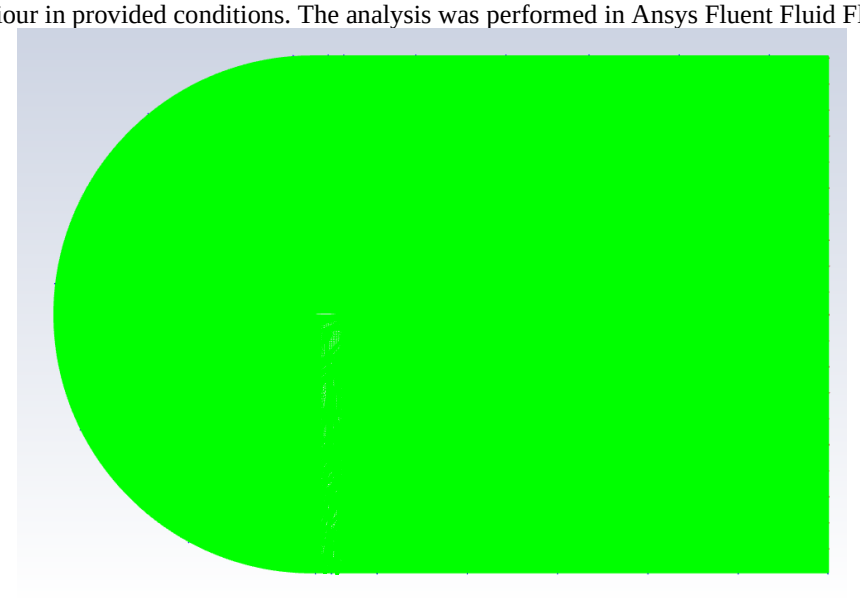


Figure 9 Generated Mesh in Ansys Fluent Fluid Flow Interface

A. Considerable Reynolds Number:

Referring to a general Reynolds Numbers whose velocity was analysed against different angle of attacks was taken into account, one being from the turbulence

region. Hence, $5x10^6$ was the most suitable and angle of attacks were chosen as 4°, 8° and 12° respectively. The adequate choice of angle of attacks proved to be sufficient in analysing the transition in lift and drag behaviour as the flow changes from potentially laminar to turbulent. For 4° AoA it was observed it to represents a low lift condition, 8° helped in creating moderate lift condition, and stalling effect started to dominate at 12°.

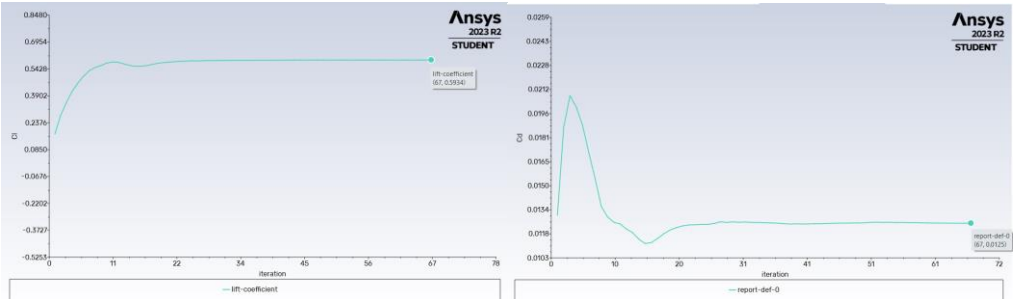


Figure 10 Lift and Drag Coefficient Values for Reynolds Number = $5x10^6$ and 4° Angle of Attack (k-ω Model)

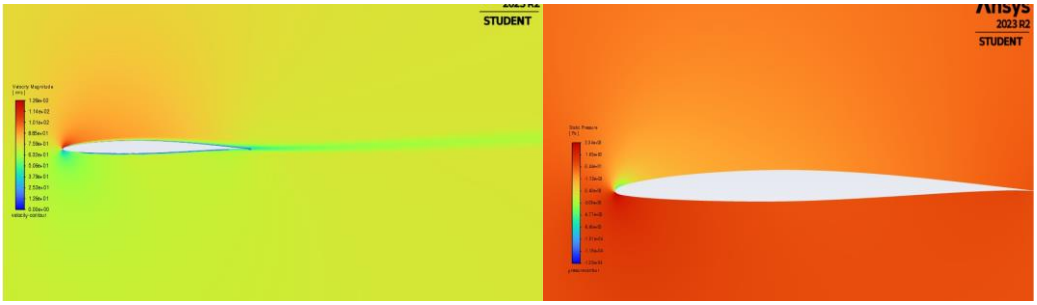


Figure 11 Velocity and Pressure Contours for Reynolds Number = $5x10^6$ and 4° Angle of Attack (k-ω Model)

Keeping in view the k-ω Turbulence Model and referring to Reynolds Number = $5x10^6$ and 4° AoA, it was observed that the low shift condition dominated on the broader perspective. The flow about the entire airfoil underwent stagnation, dominantly about the boundaries, while the velocity value peaked about the leading edge of the airfoil. It was also observed that about the trailing edge, the flow underwent slight bending, which was 4° in perfect accordance with the provided parameter. Initially the parameters were set for 1000 iterations, however convergence was observed at 67th iteration for which the values of coefficient of lift and drag were evaluated to be 0.5934 and 0.0125 respectively.

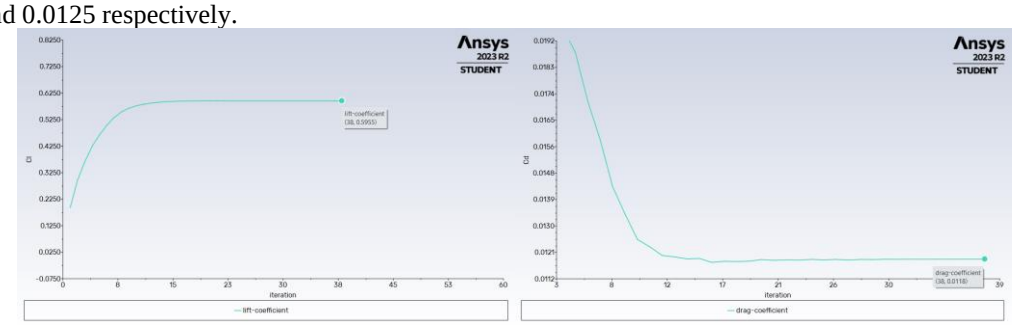


Figure 12 Lift and Drag Coefficient Values for Reynolds Number = $5x10^6$ and 4° Angle of Attack (S-A Model)

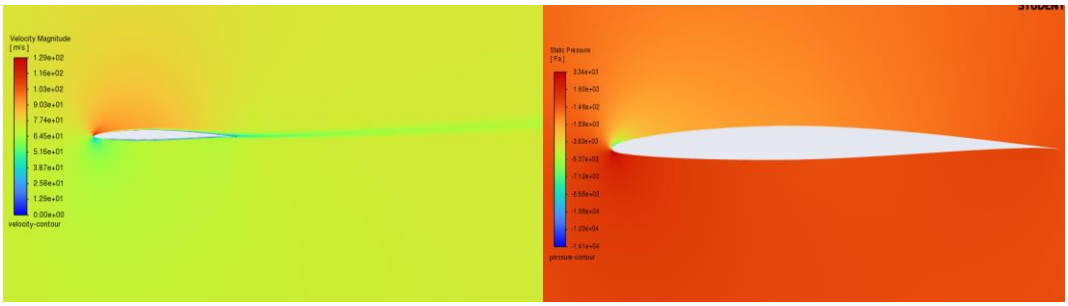


Figure 13 Velocity and Pressure Contours for Reynolds Number = $5x10^6$ and 4° Angle of Attack (S-A Model)

Keeping in view the previous example, using S-A model, it was observed that the low shift condition dominated on the broader perspective. The flow about the entire airfoil underwent stagnation, especially about the with the

velocity profile entering into state of complete stagnation about the entire airfoil. It was also observed that about the trailing edge, the flow underwent slight bending, which was 4° in perfect accordance with the provided parameter. Initially, the number of iterations were set for 1000 iterations, however convergence rate for S-A model is significantly high so the adequate readings were achieved at 38th iteration for which the values of coefficient of lift and drag were evaluated to be 0.5955 and 0.0118 respectively.

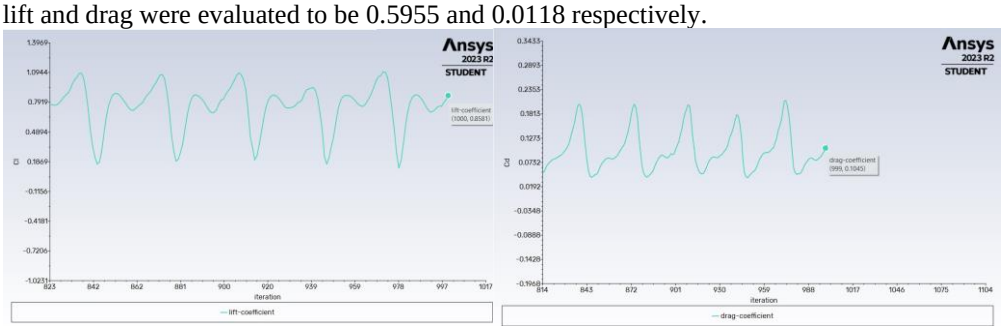


Figure 14 Lift and Drag Coefficient Values for Reynolds Number = 5x10^6 and 8°Angle of Attack (k-ω Model)

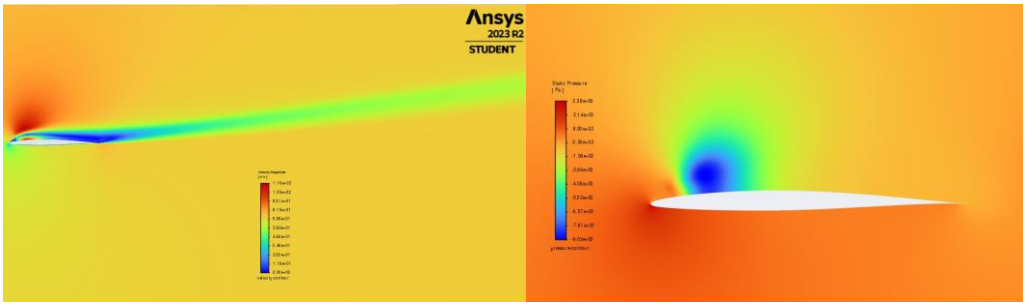


Figure 15 Velocity and Pressure Contours for Reynolds Number = 5x10^6 and 8°Angle of Attack (k-ω Model)

Referring to the choice of angle of attack, which was chosen to be 8°, the value of lift coefficient arouse to some extent and so did the drag coefficient, whose value for 1000 iterations were observed to be 0.8581 and 0.1045 respectively. As soon as the angle of attack was increased, reaching at 8°, it was observed that the flow started to bend at with the extent of stagnation having increased significantly both for the velocity and pressure distribution about the surface of airfoil blades at a higher angle of attack (8 degrees) in comparison to the 4°angle of attack. The dominant significant difference was expected to be a considerably lower pressure on the backside of the airfoil owing to a greater push at slightly higher angle of attack.

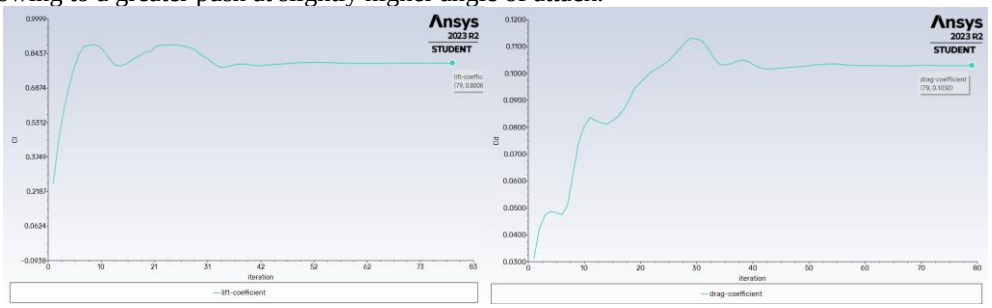


Figure 16 Lift and Drag Coefficient Values for Reynolds Number = 5x106 and 8°Angle of Attack (S-A Model)

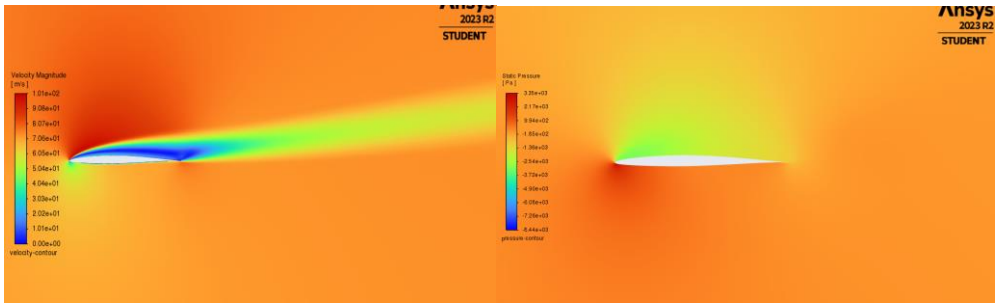


Figure 17 Velocity and Pressure Contours for Reynolds Number = 5x106 and 8°Angle of Attack (S-A Model)

The same airfoil was simulated in S-A modelling, which helped in yielding promising results as well, with great similarity to the previous one. Yet, it was observed that there was significant increase in convergence rate with

one attained at 79th iteration instead of 1000, as set forth. Stagnation about the airfoil, when analysed for the velocity profile dominated about the upper region of airfoil consistent with the results obtained in k-ω model. The values of lift coefficient and drag coefficient were 0.8006 and 0.1030 respectively.

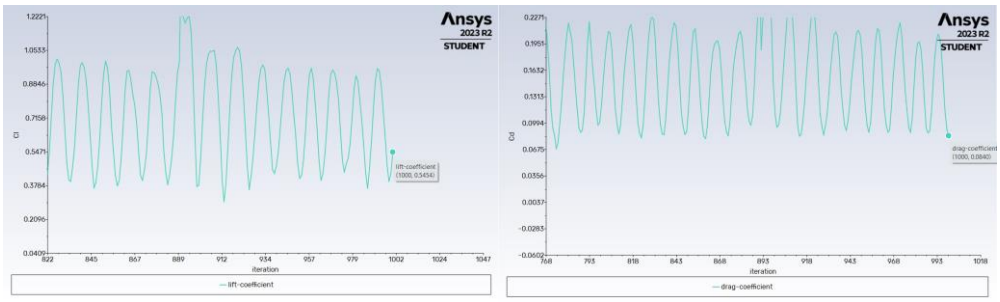


Figure 18 Lift and Drag Coefficient Values for Reynolds Number = 5x10^6 and 12° Angle of Attack (k-ω Model)

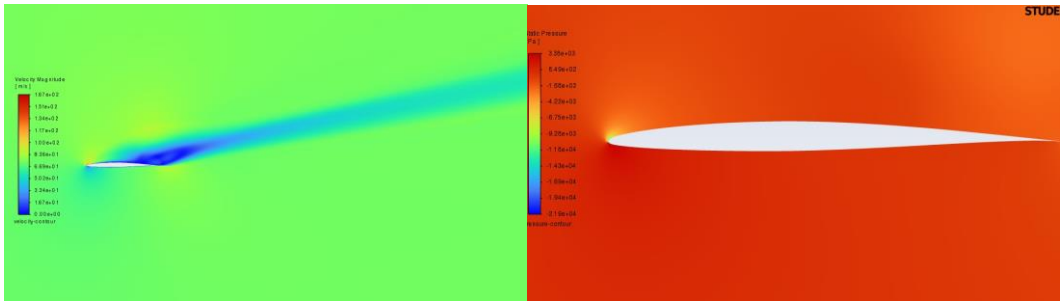


Figure 19 Velocity and Pressure Contours for Reynolds Number = 5x10^6 and 12° Angle of Attack (k-ω Model)

At 12°, the stalling began to dominate. It was specifically observed for the velocity gradient the having stagnated about the entire surface of airfoil and especially about the leading and trailing edge and particularly about the upper region of airfoil. Since the angle of attack was increased, the velocity flow underwent significant bending being dominant about the trailing edge where turbulence effects dominated. In view of pressure contour, the value of static pressure uniformly increased and distributed evenly about the surface of the airfoil. By drawing comparison for AoA's taken, respectively 4° and 8°, the extent of stagnation was observed to be maximum for the maximum angle brought into consideration, which was 12°, against which stalling effects slightly started to dominate. Moreover, referring to the computational values of lift and drag coefficients for consecutive 1000 iterations, they were evaluated to be 0.5454 and 0.0840 respectively. It is pertinent to mention that due to minute stalling effects, the values of lift and drag coefficient have decreased to a great significant value.

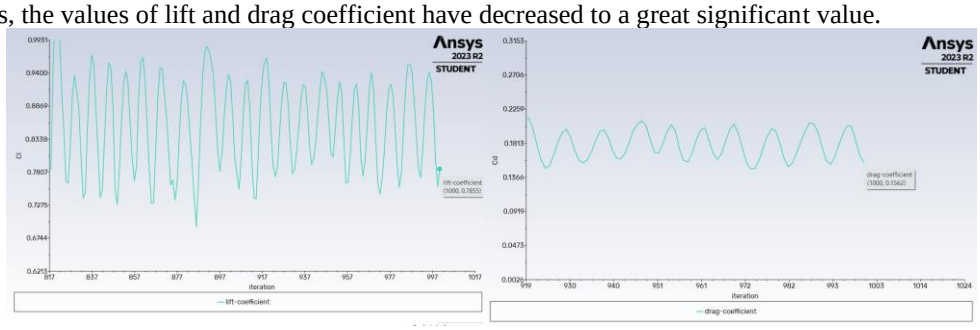


Figure 20 Lift and Drag Coefficient Values for Reynolds Number = 5x10^6 and 12° Angle of Attack (S-A Model)

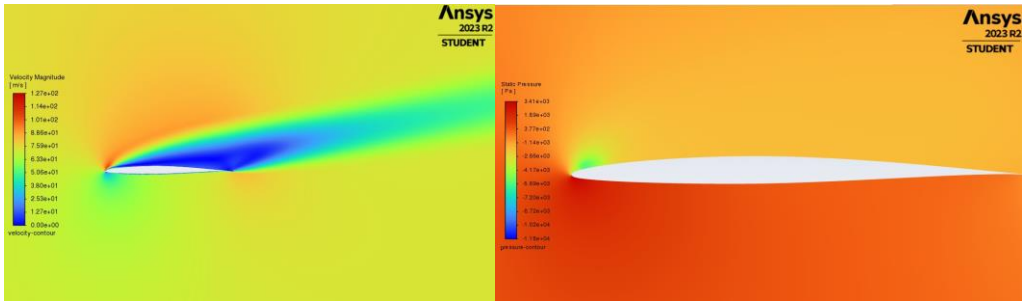


Figure 21 Velocity and Pressure Contours for Reynolds Number = 5x10^6 and 12° Angle of Attack (S-A Model)

With the S-A model, consistent results were observed, which coincided with those obtained using the k-ω turbulence modelling, with the values for lift and drag coefficient obtained as 0.7855 and 0.1562 respectively. It is pertinent to assert that the values for both have decreased significantly over the continuous iterations owing to the fact of stalling gradually dominating. The only dominant change observed for the velocity profile for both models was significantly decreased velocity over the surface surrounding the airfoil.

Table 5 Comparison Table for Values of Lift and Drag Coefficient for Considerable value of Reynolds Number

k-ω Turbulence Model				**Spalart-Allmaras Vorticity Turbulence Model**			
AoA	**C_L**	**C_D**	**Convergence Criterion** *(Iteration)*	**AoA**	**C_L**	**C_D**	**Convergence Criterion** *(Iteration)*
4°	0.5934	0.0125	67th	4°	0.5955	0.0118	38th
8°	0.8581	0.1045	1000th	8°	0.8006	0.1030	79th
12°	0.5454	0.0840	1000th	12°	0.7855	0.1562	1000th

B. Reynolds Number for Stalling Condition:

- *Stalling:*

In regard of aerodynamics and aviation, stalling is a condition for which there is a significant decrease in the value of lift coefficient value for increase in the angle of attack beyond a prescribed limit. Critical angle of attack is a specific terminology brought into consideration for an angle of attack at which the stalling dominates. The very critical angle is dependent upon the geometric parameters of airfoil or sections of analysis (like wings of aircraft), the aspect ratio etc. The typical value for the critical angle is between the range of 8 to 20 degrees relative to the incoming wind ("relative wind") for most subsonic airfoil.

For relatively small angle of attacks, the flow separation typically starts even with the attached flow about the wing/airfoil still in dominance. With the progressive increase in the value of angle of attack, the separated regions on the top of airfoil/wing increase in size and hinder the wing's ability to create lift. At the critical angle of attack, separated flow is so dominant that additional increases in angle of attack produce less lift and more drag.

Stalling maybe experienced for a fixed-wing aircraft, which consequently leads to significant change in the altitude or buffeting. Most aircraft are designed to have a gradual stall with characteristics that will warn the pilot and give him or her time to react. For example, an aircraft that does not buffet before the stall may have an audible alarm or a stick shaker installed to simulate the feel of a buffet by vibrating the stick fore and aft. The critical angle of attack in steady straight and level flight can be attained only at low airspeed. Attempts to increase the angle of attack at higher airspeeds can cause a high-speed stall or may merely cause the aircraft to climb.

- *Analysis and Choice of Parameters:*

Regarding the analysis of stalling effect, the most appropriate choice of Reynolds Number whose value is $3x10^7$, against which the possible angle of attacks have been chosen to be 8°, 12° and 16° respectively. In this regime, focus on capturing the stall behaviour. Start with 8° AoA, which might show increased lift compared to the lower Re case. Then move to 12° where stall might initiate, and finally 16° to clearly observe the significant drop in lift coefficient (C_l) due to stall.

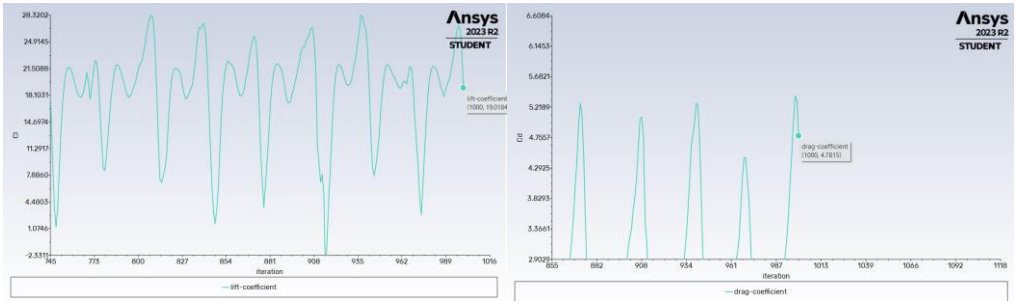


Figure 22 Lift and Drag Coefficient Values for Reynolds Number = $3x10^7$ and 8° Angle of Attack (k-ω Model)

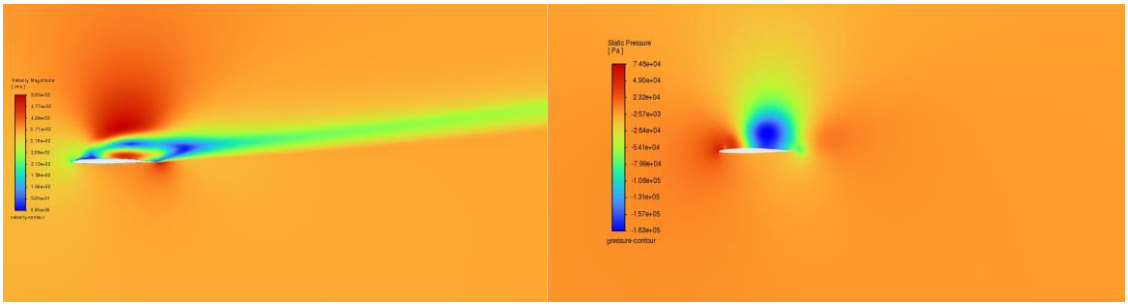


Figure 23 Velocity and Pressure Contours for Reynolds Number = $3x10^7$ and 8° Angle of Attack (k-ω Model)

Having the stalling condition brought into consideration for which a particular Reynolds number was chosen against which angles of attack were also set forth. While considering the least angle here, which was 8°, it was observed that the effects of stalling were somewhat not quite dominant. Due to the choice of angle, it was observed especially for the velocity contour that the flow swayed about the trailing edge, while ensuring stagnation to be significant about the very region and the surface of airfoil. Regarding the pressure contour, negative pressure concentration dominated above the upper region of airfoil which asserted the fact that due to rather greater value of angle of attack, flow separation slightly dominated above the region. Bringing into perspective the lift and drag coefficients, the values came out to be 19.0184 and 4.7815 respectively.

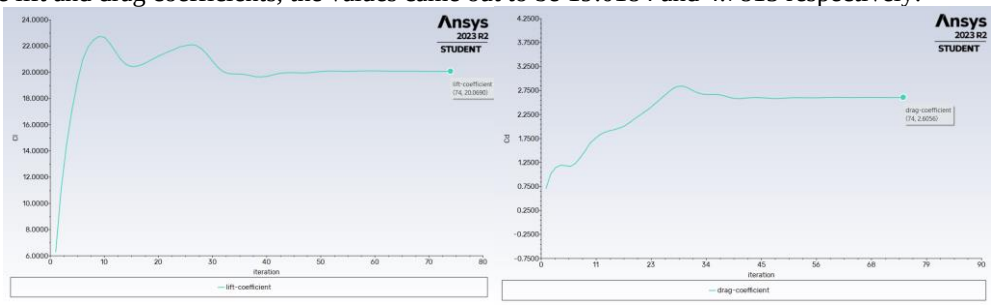


Figure 24 Lift and Drag Coefficient Values for Reynolds Number = $3x10^7$ and 8° Angle of Attack (S-A Model)

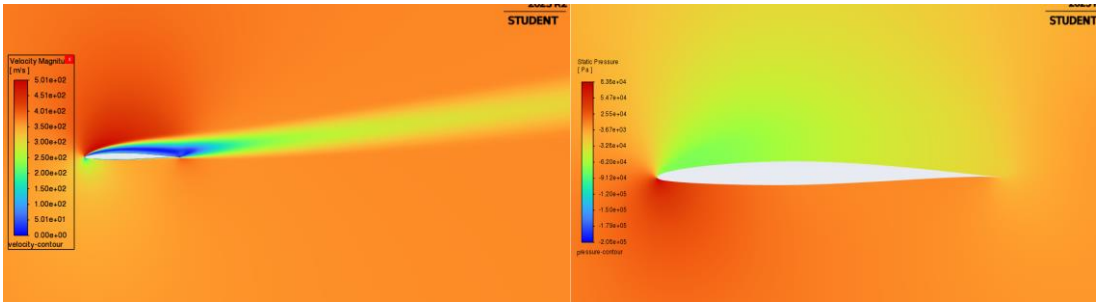


Figure 25 Velocity and Pressure Contours for Reynolds Number = $3x10^7$ and 8° Angle of Attack (S-A Model)

Analysing for S-A Vorticity model, it was observed for 1000 repetitive iterations, the values of lift and drag coefficient came out to be 20.0690 and 2.6056 respectively, for 74 iterations. Yet it was pertinent to mention that the behaviour of stalling was concordant to one observed for the k-ω model, yet the only dominant difference between the two existed for the airfoil stagnation extent, which was uniform when the velocity profile was concerned, yet for the pressure profile, throughout negative pressure dominated about the upper region of airfoil.

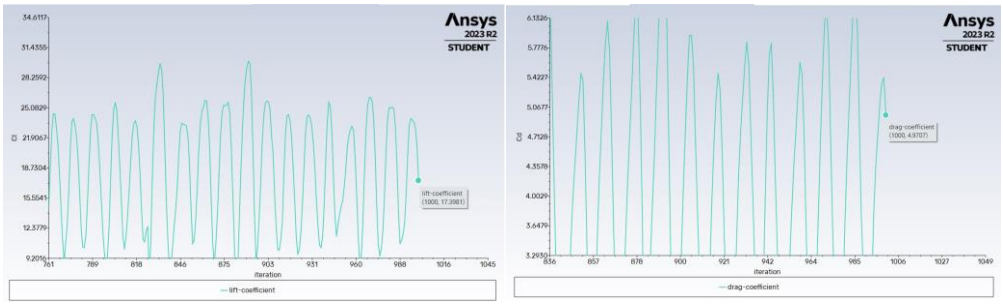


Figure 26 Lift and Drag Coefficient Values for Reynolds Number = $3x10^7$ and 12° Angle of Attack (k-ω Model)

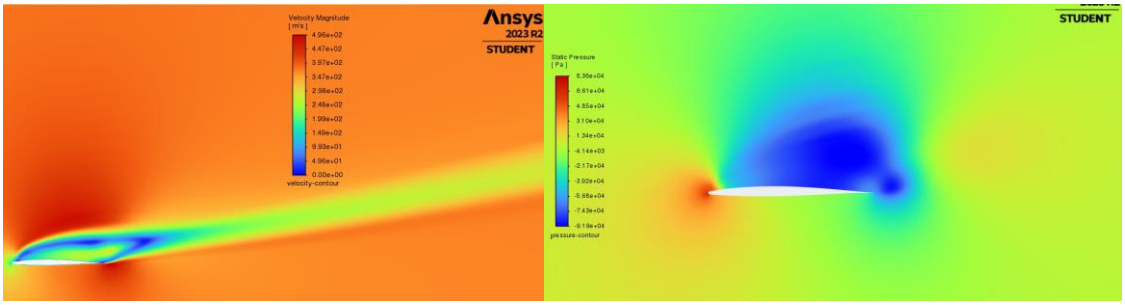


Figure 27 Velocity and Pressure Contours for Reynolds Number = 3x10^7 and 12°Angle of Attack (k-ω Model)

Upon increasing the angle of attack to 12°, the stalling effects started to slightly dominate with the velocity distribution about the trailing edge having undergone significant stagnation and the flow tilted 12° upward from the origin. Visualizing the stalling effect, it can be observed dominantly above the trailing edge, with the velocity having concentrated about that region. It was also observed for the pressure contour that the extent of stagnation had increased significantly and has evenly distributed about the leading edge of the airfoil's surface, while the distribution of static pressure about the entire contour was rather uniform and symmetric. The flow separation was comparatively more than the previous case hence abiding to the fact that some stalling had indeed taken place, yet the effects were still not dominant. Bringing into perspective the lift and drag coefficients, the values came out to be 17.3981 and 4.9707 respectively. The decrease in the value of lift coefficient meant that stalling had started to dominate.

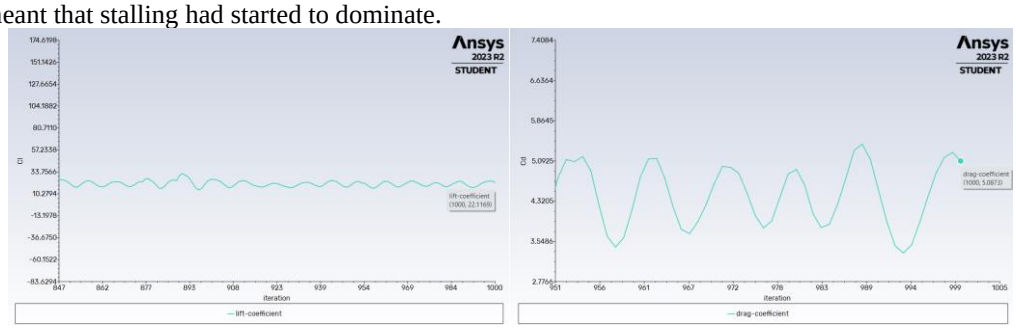


Figure 28 Lift and Drag Coefficient Values for Reynolds Number = 3x10^7 and 12°Angle of Attack (S-A Model)

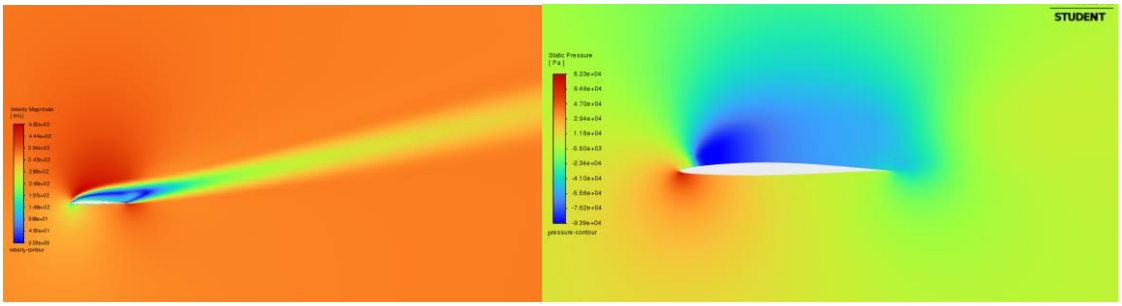


Figure 29 Velocity and Pressure Contours for Reynolds Number = 3x10^7 and 12°Angle of Attack (S-A Model)

Analysing the stalling effect for the set Reynolds Number at 12° in S-A model, the values of lift and drag coefficient for 1000 consecutive repetitive iterations yielded 22.1169 and 5.0873 respectively, which slightly deviated in value from those observed in k-ω turbulence model. As far as stalling effect was concerned, it was somewhat dominant in the case with maximum stagnation above the airfoil region in uniform distribution. Due to the uniformity of the velocity distribution, it was evident that negative pressure was concentrated over the entire region. At the leading edge, the value of pressure rose to maximum value which somewhat ensured that the stalling had started to dominate.

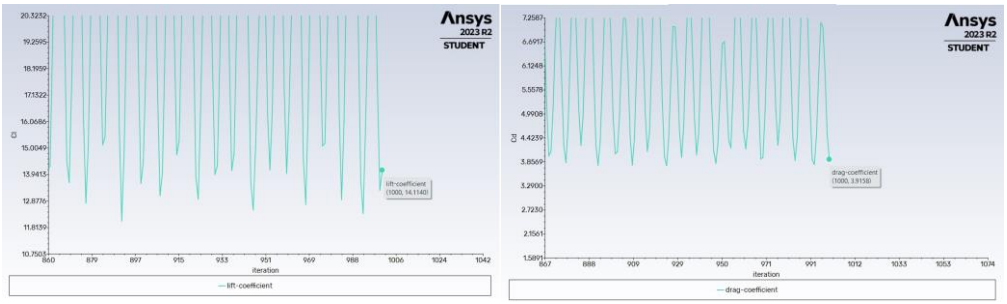


Figure 30 Lift and Drag Coefficient Values for Reynolds Number = 3x10^7 and 16° Angle of Attack (k-ω Model)

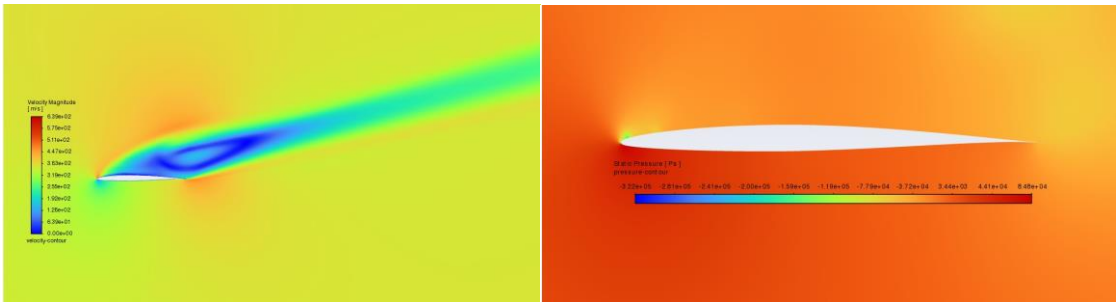


Figure 31 Velocity and Pressure Contours for Reynolds Number = 3x10^7 and 16° Angle of Attack (k-ω Model)

In perfect accordance with the discussion, it was concluded that the stalling occurs for a maximum angle of attack, being referred to as the critical angle of attack, which was 16° for the aforementioned case. It was dominantly observed that the stalling had taken into account, and the velocity distribution about the entire contour was messed up. The velocity contours illustrated the airflow separation over the upper part of the airfoil near the leading edge, with airflow reattaching further downstream or remaining separated entirely. Such flow separation served the purpose in disrupting the pressure distribution and significantly reduced the lift generation. The pressure contour indicated a region of low pressure over the upper surface of the airfoil near the leading edge, followed by a sharp increase in pressure towards the trailing edge. In the generation of lift, the pressure difference served a significant role. However, at high angles of attack, which was 16° for the aforementioned case, the flow underwent separate from the airfoil surface, reducing that uniform pressure distribution and consequently stalling. The values of lift and drag coefficient for 1000 iterations came out to be 14.1140 and 3.9158 respectively.

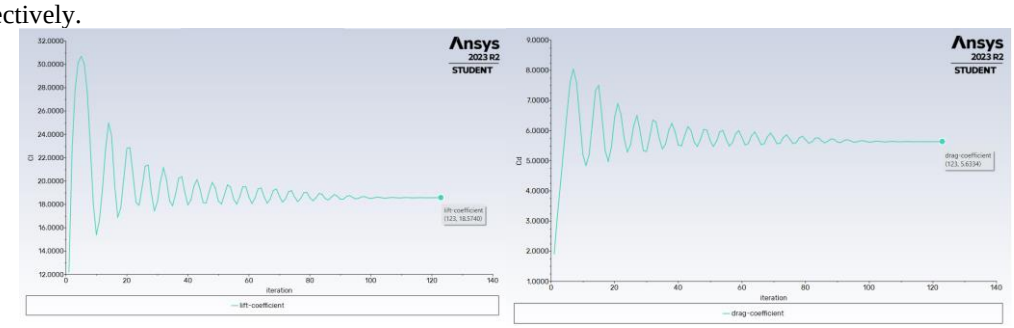


Figure 32 Lift and Drag Coefficient Values for Reynolds Number = 3x10^7 and 16° Angle of Attack (S-A Model)

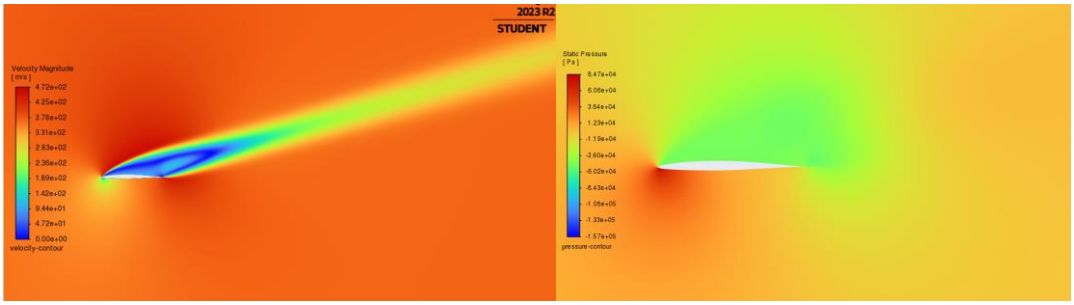


Figure 33 Velocity and Pressure Contours for Reynolds Number = 3x10^7 and 16° Angle of Attack (S-A Model)

Generally, as discussed before, stalling effects come into dominance as angle of attack increases in value. The afore discussed airfoil was simulated in S-A model to observe behaviour of angle of attack on velocity and,

hence stalling. It was observed that the velocity magnitude about the leading and trailing edges of airfoil was greater as compared to modelling done in k-ω setup, however it was observed that the convergence rate was significantly high when analysed in S-A modelling setup, where convergence for the values for lift and drag coefficient was observed at 123rd iteration with values 18.5740 and 5.6334 respectively.

Table 6 Comparison Table for Values of Lift and Drag Coefficient for Stalling value of Reynolds Number

k-ω Turbulence Model				**Spalart-Allmaras Vorticity Turbulence Model**			
AoA	**C_L**	**C_D**	**Convergence Criterion** *(Iterations)*	**AoA**	**C_L**	**C_D**	**Convergence Criterion** *(Iterations)*
8°	19.0184	4.7815	1000th	8°	20.0690	2.6056	74th
12°	17.3981	4.9707	1000th	12°	22.1169	5.0873	79th
16°	14.1140	3.9158	1000th	16°	18.5740	5.6334	123th

C. Reynolds Number for Shockwave Condition:

- *Shockwave:*

Shockwave is a type of propagating disturbance that moves faster than the local speed of sound in the medium. Shockwave is actually an energy carrier, quite similar to a normal wave and can propagate through a medium but is characterized by an abrupt, nearly discontinuous, change in pressure, temperature, and density of the medium. Unlike ordinary sound waves, the speed of a shock wave varies with its amplitude. The speed of a shock wave is always greater than the speed of sound in the fluid and decreases as the amplitude of the wave decreases. When the shock wave speed equals the normal speed, the shock wave abolishes and is reduced to a typical sound wave.



Figure 34 Typical Shockwave created by Supersonic jet

A typical shockwave can actually be treated as a discontinuity where significant increase can be observed for entropy value from the region where the shock passes Since no fluid flow is discontinuous, a control volume is established around the shock wave, with the control surfaces that bound this volume parallel to the shock wave (with one surface on the pre-shock side of the fluid medium and one on the post-shock side). The two surfaces are separated by a very small depth such that the shock itself is entirely contained between them. At such control surfaces, momentum, mass flux and energy are constant; within combustion, detonations can be modelled as heat introduction across a shock wave.

- *Analysis and Adjustment of Parameters:*

For obtaining the optimum results especially for analysing the shockwave behaviour, significantly high value of Reynolds Number, about $1x10^8$ is taken into account while keeping the angle of attack as less as possible. Considering the following case for convenient purpose, the optimum Reynolds number selected was $1x10^8$ with angle of attacks respectively as 2°, 4°, and 6° respectively. At high Re, even small AoA can cause supersonic flow near the leading edge. Choose 2° for a nearly symmetric flow, 4° to see the initial shock formation, and 6° for a stronger shock. It was observed that k-ω Turbulence model did not help in producing promising results hence in lieu of provided parameters, the S-A turbulence model was adopted for the analysis. Modelling the shockwave case in ideal conditions in both aforementioned models yielded no conclusive results, so the model was changed from ideal gas to real gas, for

which the fluid (air) was accounted for as real gas, for whom the working temperature was 298 K instead of normal 303 K.

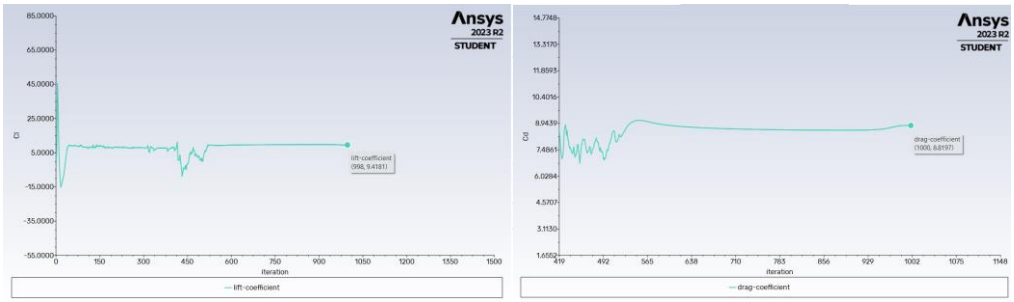


Figure 35 Lift and Drag Coefficient Values for Reynolds Number = 1x10^8 and 2°Angle of Attack (k-ω Model)

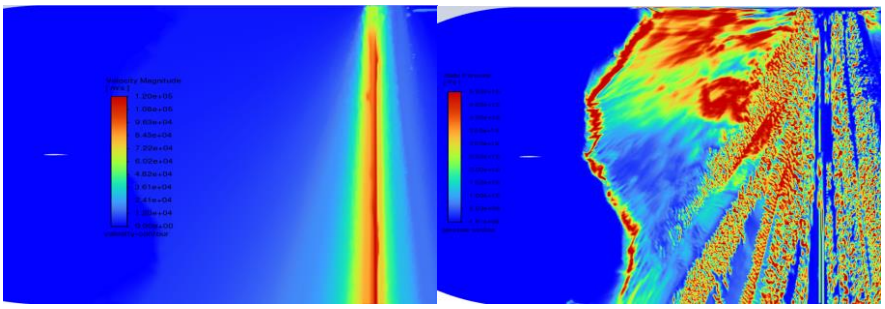


Figure 36 Velocity and Pressure Contours for Reynolds Number = 1x10^8 and 2°Angle of Attack (k-ω Model)

In lieu of the parameters set forth for analysis of the airfoil using k-ω turbulence model, it is obvious from Figure 36 that dispersion is quite evident with no evidence of shockwave being generated. It is pertinent to assert that the SST model generally brings into use the limiter which plays an important role in preventing extreme production of turbulence. It helps in keeping the turbulence levels within acceptable level. However, there are some regions where the strong shockwaves and adverse pressure gradients can lead to some restrictions and hence causing suppression of the entire model, a valid reason to justify for dispersion within the contours for pressure and velocity. Due to the strong underestimation of turbulence, it significantly affects the accuracy of the simulation.

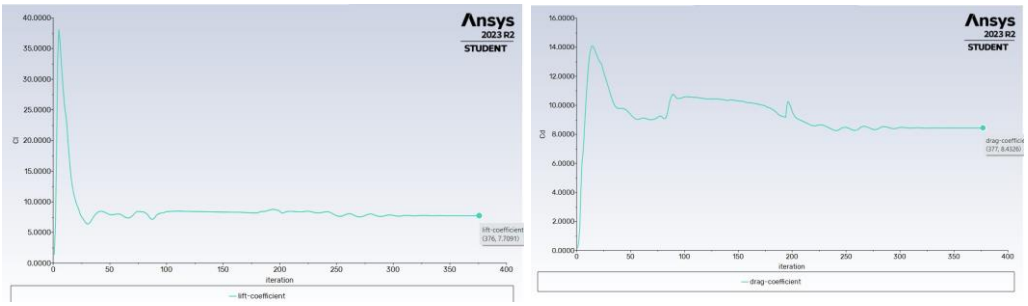


Figure 37 Lift and Drag Coefficient Values for Reynolds Number = 1x10^8 and 2°Angle of Attack (S-A Model)

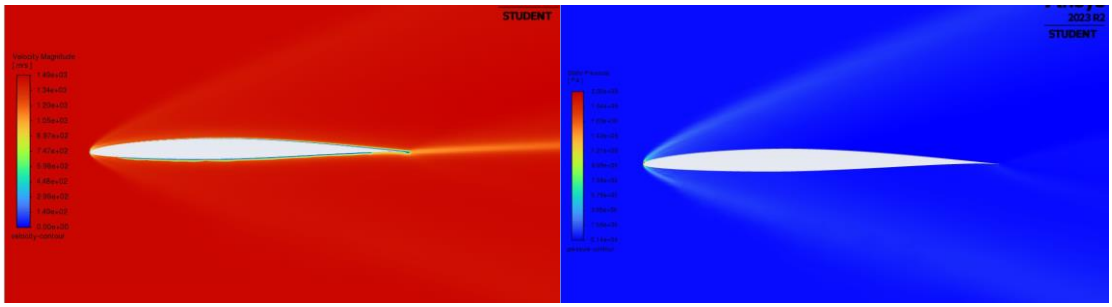


Figure 38 Velocity and Pressure Contours for Reynolds Number = 1x10^8 and 2°Angle of Attack (S-A Model)

Analyzing for S-A Vorticity model, which itself proved best for analyzing the shockwave. It was observed for initally parameterized 1000 iteartiosn, the convergence was observed at 377th iteration for which the values of lift and drag coefficient came out to be 7.7091 snd 8.4326 respectively.The shockwave was observed to dominate about the leading edge of the airfoil, for which a sudden spike in the pressure concentartion was

observed. As from the color scheme given it was observed that the value of pressure about the leading trail was 2.06×10^6 Pa, which was quite a significant value.

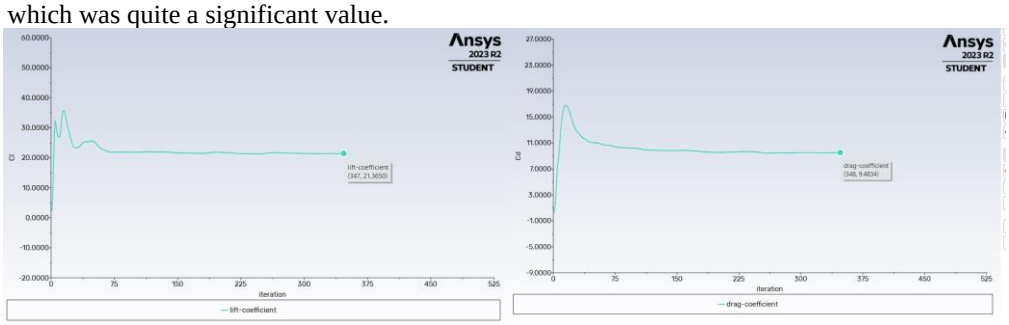


Figure 39 Lift and Drag Coefficient Values for Reynolds Number = 1×10^8 and 4°Angle of Attack (k-ω Model)

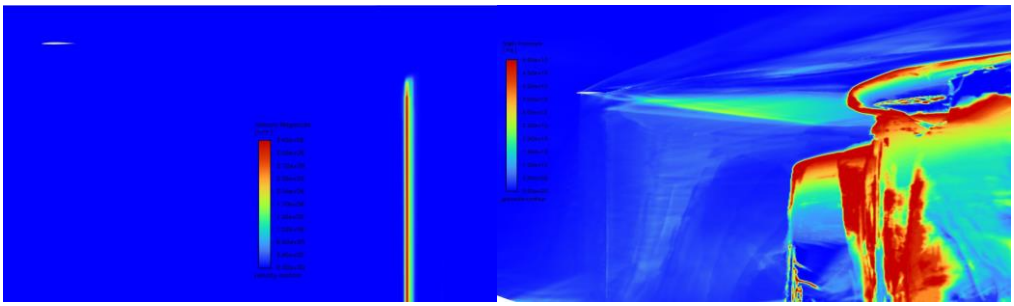


Figure 40 Velocity and Pressure Contours for Reynolds Number = 1×10^8 and 4°Angle of Attack (k-ω Model)

Analysis of shockwave using k-ω turbulence model provided no valuable information, as detailed from the Figure 40, where dispersion and irregularities had dominated the analysis. From the pressure contour, it was maintained that minute extent of shockwave can be observed just above the leading edge, from which spike in pressure value has strengthened the mentioned discussion that shockwave has been generated. Since no valuable information could be sought from k-ω turbulence model, the only resort to analyse was the S-A model which is discussed below.

Referring to the non-provision of valuable information using k-ω turbulence model, it takes into account the freestream properties (which are the flow conditions being far upstream of the shock) within the calculations. Such dependency of freestream condition proves to be otherwise problematic for shockwaves due to the fact that the flow characteristics change undergo sudden changes within the shock region. Such freestream conditions accurately might not properly represent the flow behaviour right behind the shock, hence causing inaccurate predictions within the concerned critical area.

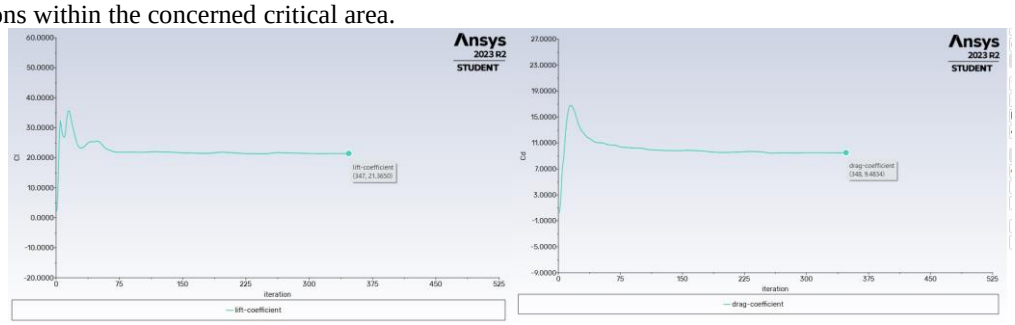


Figure 41 Lift and Drag Coefficient Values for Reynolds Number = 1×10^8 and 4°Angle of Attack (S-A Model)

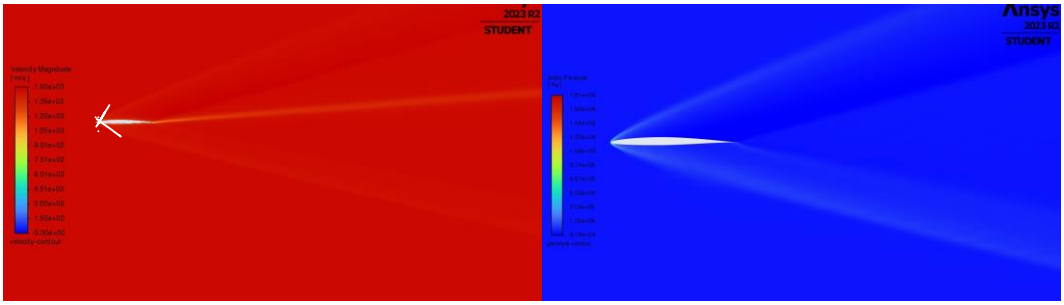


Figure 42 Velocity and Pressure Contours for Reynolds Number = 1×10^8 and 4°Angle of Attack (S-A Model)

It was observed that again the shockwave was only properly observed when the S-A Vorticity model was taken into account. Analysing for angle of attack as 4°, it was observed that the width of shockwave was significantly greater than the previous case where the angle of attack was chosen to be 2°. Referring to the velocity profile, maximum uniform velocity distribution was observed within the entire contour, with the value of velocity slightly decreasing as the flow swayed about the trailing edge (due to the choice of angle of attack). In lieu of parameters set forth, the results seemed to be concordant with the real data values. Owing to the fact convergence rate of S-A model, the values of lift and drag coefficients converged at 348th iteration instead of regular 1000th iteration, and the values came out to be 21.3650 and 9.4838 respectively. Another fact to support the shockwave was the sudden rise in value of pressure gradient about the leading edge of airfoil, for which the pressure was 1.81x10^{6} Pa.

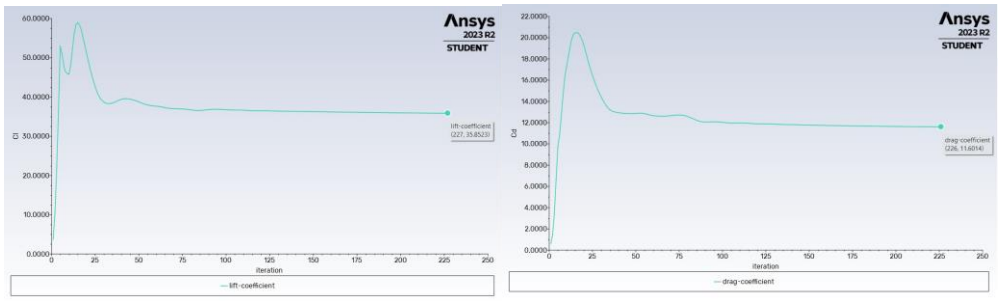


Figure 43Lift and Drag Coefficient Values for Reynolds Number = 1x10^{8} and 6°Angle of Attack (k-ω Model)

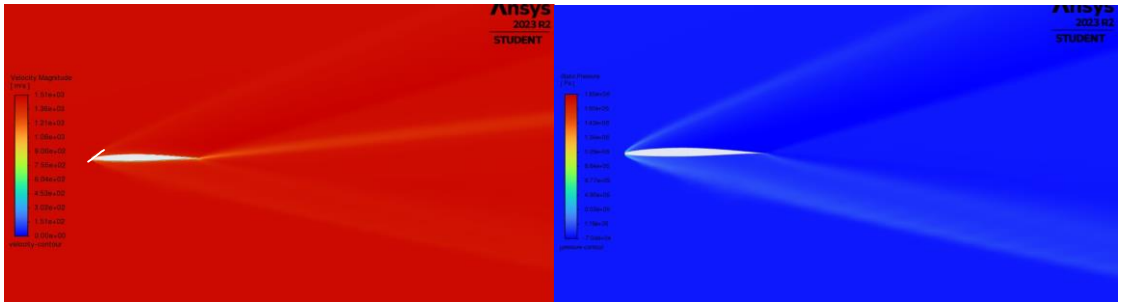


Figure 44 Velocity and Pressure Contours for Reynolds Number = 1x10^{8} and 6°Angle of Attack (k-ω Model)

At 6° angle of attack for k-ω turbulence model, shockwave was observed and the values of lift and drag coefficient at 227th iteration came to be 35.8523 and 11.6014 respectively, while originally the model was set for 1000 iterations. It was pertinent to mention that 6° was the only angle of attack for which the k-ω turbulence model helped in yielding some valuable information. Analysis revealed that the k-ω model is generally established to analyse the macro properties of material in an effective manner and also it was established that the aforementioned model was comparatively complex as far as establishment was concerned. From both the velocity and pressure contour, the shockwave was visibly dominant. It was observed for velocity contour, that maximum velocity was distributed uniformly about the entire contour and since the angle of attack was 6°, the flow separation was also observed due to which there was a decrease in value of velocity about the very region. Coming to the pressure contour, due to uniform maximum velocity contribution, the static pressure was also observed to be distributed in a uniform manner. The width of shockwave was observed to be the maximum from the above two cases analyzed from which a conclusion was drawn that the width of shockwave increased significantly as the angle of attack increased by and by.

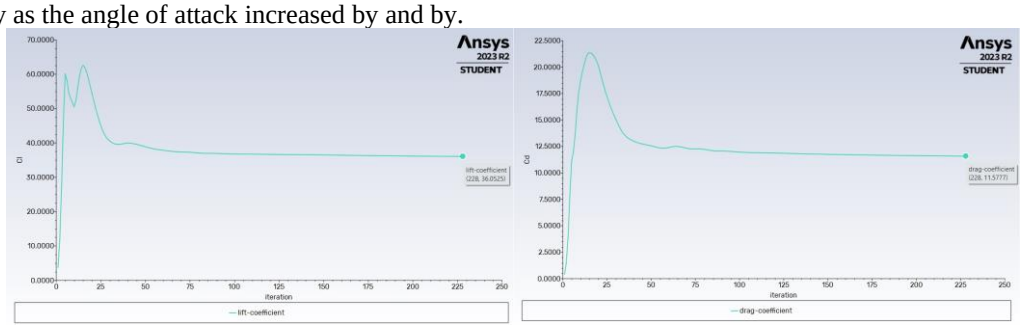


Figure 45 Lift and Drag Coefficient Values for Reynolds Number = 1x10^{8} and 6°Angle of Attack (S-A Model)

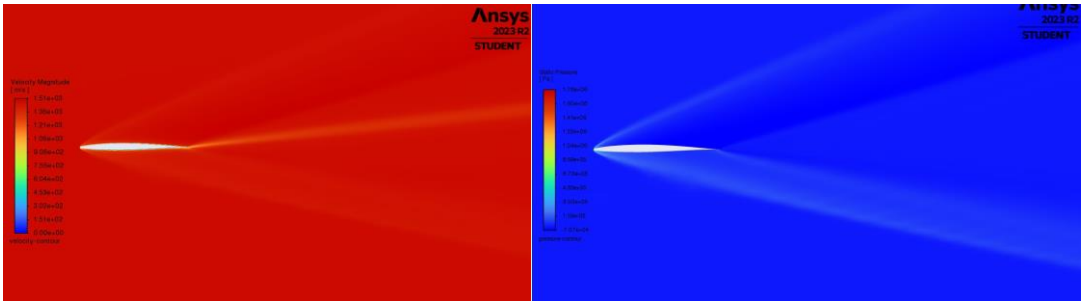


Figure 46 Velocity and Pressure Contours for Reynolds Number = $1x10^8$ and 6° Angle of Attack (S-A Model)

Analysing for the scenario in Spalart-Allmares model, at 6° angle of attack, the shockwave was observed and the values of lift and drag coefficient at 228th iteration came to be 36.0525 and 11.5777 respectively, while originally the model was set for 1000 iterations. From the Figure 43 and 45, it was observed that the convergence rate for both the scenarios remained the same, having one attained at the aforementioned figure (228th iteration). From both the velocity and pressure contour, the shockwave was visibly dominant. It was observed for velocity contour, that maximum velocity was distributed uniformly about the entire contour and since the angle of attack was 6°, the flow separation was also observed due to which there was a decrease in value of velocity about the very region. Coming to the pressure contour, due to uniform maximum velocity contribution, the static pressure was also observed to be distributed in a uniform manner. The width of shockwave was observed to be the maximum from the above two cases analyzed from which a conclusion was drawn that the width of shockwave increased significantly as the angle of attack increased by and by.

Table 7 Comparison Table for Values of Lift and Drag Coefficient for Shockwave value of Reynolds Number

k-ω Turbulence Model				**Spalart-Allmaras Vorticity Turbulence Model**			
AoA	**C_L**	**C_D**	**Convergence Criterion** *(Iterations)*	**AoA**	**C_L**	**C_D**	**Convergence Criterion** *(Iterations)*
2°	9.4181	8.8197	1000th	2°	7.7071	8.4326	377th
4°	21.3650	21.3650	348th	4°	21.3650	21.3650	348th
6°	35.8523	11.6014	227th	6°	36.0525	11.5777	228th

IX. Discussions Regarding Analysis

The following document adequately addresses the CFD analysis of NACA 64A-206 airfoil, which is quite symmetrical to NACA 64A-204, being employed in F-16 aircrafts and other high speed testing crafts. The analysis was performed for three different cases for which three different values of Reynolds numbers were taken into account, respectively for normal conditions, stalling conditions, and shockwave production conditions. It is pertinent to mention that two different models, respectively as SST k-ω Turbulence model and S-A Vorticity turbulence model were taken into account in order to compare the results obtained using both models. Owing to the meshing conditions, it could not be adequately mastered for because of choice of airfoil and computation conditions. The normal and stalling cases were successfully analysed using both the aforementioned turbulence models, yet it was impossible to obtain adequate results for shockwave case using k-ω turbulence model at relatively small angles due implication of freestream conditions which undergo sudden change within the shockwave case, rendering the analysis useless. Moreover, due to suppression of turbulence renders dispersion within the generated model for velocity and pressure causes such scenarios to come into dominance. The values of lift and drag coefficient observed using both models, however some values contributed some similarity with the numerical values present in the datasheets for the different airfoils.

X. Conclusions

In conclusion it is pertinent to mention that CFD plays an integral role in fields and applications, primarily linked to mechanical and aerospace engineering, having simplified, and replaced the tedious analysis techniques which involved rigorous deliberation on graphing, testing etc. Airfoils serve as primary model for different aerodynamic designs, having the ability to generate significantly large value of lift and drag forces at relatively small angles of attack, being predominant for four-digit airfoils. Appropriate CFD analysis helps in optimization of designs, greater working efficiency and improving speed, especially where the aerodynamic designs are concerned. It also helps in preventing disasters that might be evident owing to improper designing.

The main goal of the analysis was to observe the behavior of NACA 64A-206 airfoil in supersonic conditions, an airfoil which itself or its modifications are used on interceptors and supersonic fighter jets, predominantly F-

16. The research established concordant relations for the varying of lift and drag coefficients owing to interchanging of angle of attacks. The analysis was brought into consideration using both the k-ω turbulence model and Spalart-Allmaras turbulence modelling, from which it was observed that the S-A model proved to be more reliable and effective owing to fast convergence rate and less computational costs with greater accuracy. The airfoil was subjective to three different conditions, namely for the normal, stalling and shockwave cases, for which the angles of attacks were chosen between 0° and 16°, and the Reynolds numbers chosen between $5x10^6$ and $1x10^8$. It is pertinent to mention that the values for lift and drag coefficient have varied from the original model, which themselves depend upon meshing aspects. Explicitly for the shockwave case, the k-ω turbulence modelling failed to yield appropriate results owing to limitations of analysis which are beyond the scope of analysis.

REFERENCES

[1] R. Carmichael, "Appendix III - 6A-Series Sections- NACA Section 64A206," Public Domain Aeronautical Software, 18th October 2018. [Online]. Available: https://www.pdas.com/sections6a.html#s64A204.

[2] Yunus A. Cengel, John M. Cimbala, Textbook on Fluid Mechanics, Tata McGraw Hill Publication, 2014.

[3] A. Wood, "Introduction to Aircraft Airfoil Aerodynamics," Aero Toolbox, 18th May 2022. [Online]. Available: https://aerotoolbox.com/intro-airfoil-aerodynamics/.

[4] C. CFD, "The Importance of Meshing in CFD and Structural FEA," Cadence, [Online]. Available: https://resources.system-analysis.cadence.com/blog/msa2022-the-importance-of-meshing-in-cfd-and-structural-fea.

[5] ANSYS, Inc. Ansys help manual. Canonsburg, Pennsylvania, USA: Ansys, 2021.

[6] Clancy, L.J., Aerodynamics, Section 5.7

[7] Anderson, John D. Jr. (January 2001) [1984], Fundamentals of Aerodynamics (3rd ed.), McGraw-Hill

[8] "The Spalart-Allmaras Turbulence Model," NASA Langley Research Center: Turbulence Modeling Resource, [Online]. Available: https://turbmodels.larc.nasa.gov/spalart.html.

[9] "NACA 64-206," Airfoil Tools, [Online]. Available: http://airfoiltools.com/airfoil/details?airfoil=naca64206-il.

[10] T. P. Hypertextbook, "Shock Waves," The Physics Hypertextbook, [Online]. Available: https://physics.info/shock/.

[11] S. a. A. Tutor, "Ansys Fluent Tutorial NACA Airfoil Analysis," YouTube, 24 May 2020. [Online]. Available: https://www.youtube.com/watch?v=d4l2ky6EEjo&t=1s.

[12] engineering-content, "Simulating NACA 2412 Airfoil over Varied Angles of Attack in Ansys Fluent with Verification," YouTube, 27 March 2024. [Online]. Available: https://www.youtube.com/watch?v=VYuouGKd1-Q.

[13] C. Thomas, "NACA2412 Tutorial in ANSYS Fluent (Student Version) - Lift, Drag, Angle of Attack," YouTube, 6th March 2023. [Online]. Available: https://www.youtube.com/watch?v=3i9Ryq-m1HA&t=1427s.

[14] O. School, "CFD analysis of an airfoil for different AoA and Calculation of lift, drag force, coefficient also," YouTube, 2nd August 2022. [Online]. Available: https://www.youtube.com/watch?v=z-qi8L-WVYM.

[15] C. Ninja, "Ansys Fluent - Compressible Flow Tutorial," YouTube, 9th April 2019. [Online]. Available: https://www.youtube.com/watch?v=YfsPxn9_3fA.

[16] K. K. N. LEO MATAK, "CFD Analysis of F-16 Wing Airfoil Aerodynmaics in Supersonic Flow," ResearchGate, Zagreb, 2022.

[17] D. V. V. K. Nataraj Kuntoji, "CFD Analysis of Tapered Wing with NACA 64-210 at the Tip and NACA 64-215 at the Root," International Journal of Science and Research (IJSR), vol. XI, no. 11, pp. 315-320, 2022.

[18] M. V. N. S. M. S. V. V. S. P. Y Seetha Rama Rao, "CFD simulation of NACA airfoils at various angles of attack," in IOP Conference Series: Materials Science and Engineering, India, 2022.

[19] H. S. A. E. Q. H. Farhan L. Rashid, "Numerical study of the air flow over modified NACA 2412 airfoil using CFD," in AIP Conference Proceedings, Iraq, 2022.

[20] M. N. M. Karansinghdangi, "CFD Analysis of an Aircraft delta wing," International Research Journal of Engineering and Technology (IRJET), vol. III, no. 12, pp. 555-560, 2016.

[21] A.-e. N. M. R. Nasser Eddegdag, "Investigation of viscous supersonic laminar flows around F-16 airfoil: Experimental, numerical, and analytical approaches," in IOP Publishing: Physics Spectra, Merrakech, 2023.

[22] C. S. A.-M. S. A. B. Marcel Blind, "Numerical and Experimental Investigation of a NACA 64A-110 Airfoil in Transonic Flow Regime," Aachen, Stuttgart, 2023.